Oxidation and Oxygen Diffusion in Ti–6al–4V Alloy: Improving Measurements During Sims Analysis by Rotating the Sample

Dominique Poquillon · Claude Armand · Julitte Huez

Abstract Titanium alloys are attractive to the industrial world, as they offer the benefits of low density, great corrosion resistance, and relatively good strength, making them viable candidates for a multitude of applications. However, above 500 °C, oxidation and oxygen diffusion in titanium alloys need to be taken into account as they change their microstructure and then their mechanical properties. Oxidations were carried out between 600 and 750 °C on a specific titanium alloy: an α–β annealed Ti–6Al–4V. Oxidation kinetics and oxygen diffusion in the matrix were studied. SIMS analyses were realized on rotating specimens of this two-phase polycrystalline alloy in order to reduce roughness. Composition profiles along the sample thickness were compared to microhardness measurements. SIMS mappings were realized on the smooth slopes of the crater.

Keywords SIMS · Ti–6Al–4V · Oxidation · Oxygen diffusion

Introduction

The market for titanium and its alloys has been increasing for 50 years and owes its success to titanium alloys outstanding technological qualities. With a low density

D. Poquillon (✉) · J. Huez
Université de Toulouse, CIRIMAT, INPT-ENSIACET, 4 Allée Emile Monso, BP 44362,
31030 Toulouse Cedex 4, France
e-mail: Dominique.Poquillon@ensiacet.fr

J. Huez
e-mail: Julitte.Huez@ensiacet.fr

C. Armand
Université de Toulouse, Service SIMS, INSA, 135 Avenue de Rangueil,
31077 Toulouse Cedex, France
e-mail: Claude.Armand@insa-toulouse.fr

(60 % of that of steel with $\rho = 4.5$ g/cm^3), excellent mechanical properties up to a temperature of about 600 °C and an exceptional corrosion resistance in many aggressive environments (sea water, human body,…), titanium alloys are widely used in the medical engineering, the chemical industry and the aerospace sector [1]. If below 300 °C some composite materials have higher specific strength than titanium alloys, at higher temperature, it is no longer the case and titanium alloys are particularly attractive.

But the use of these alloys is often limited to temperatures below 600 °C because of their oxidation behavior and of the migration of oxygen. In fact, titanium and its alloys have a strong affinity with oxygen, as in a minus manner with nitrogen, [2, 3]. Oxygen diffusion also improves poor wear properties of titanium alloys [1], but most of the time, and particularly in aircraft applications, oxidation and oxygen diffusion in titanium alloys are problematic as they impact the microstructure and thus the mechanical properties of the alloy: the alphagen element oxygen promotes the formation of an oxygen-rich Ti hexagonal solid solution (α-phase) and modifies the phase structure near the surface [3–7]. The research for improving the oxidation resistance of titanium based alloys by various surface treatments and protective coatings has been very active and is stimulated by the need to enhance both the durability and the engine performance in aerospace industry [1, 8–12]. However, numerous components are used without any coating. Additionally, for some applications oxidation may occur during stress relief heat treatment or during processing since components in titanium alloys are hot formed or machined.

A lot of studies have been devoted to these topics at temperatures met during heat treatment or representative of titanium parts service conditions [4, 13–27]. In the present study, short oxidation durations—varying from 3 to 6 h—were carried out under air between 600 and 750 °C on the most used titanium alloy: Ti–6Al–4V. Our investigations crosses thermo gravimetric results and SIMS measurements, in order to characterize the oxide layer formed under these conditions and the subsurface modified alloy layer which are often removed by machining or chemical treatments. The paper is divided into two main parts. First part focuses on the oxide scale, and second part on the oxygen dissolution into the matrix.

Materials and Experimental Procedure

Composed of 6-aluminum, 4-vanadium and the balance titanium, Ti–6Al–4V is the most common alloy of the titanium industry. It is an alpha beta titanium alloy with a good compromise between strength and toughness, and stress stability at high temperatures. Its chemical composition is given in Table 1.

Table 1 Chemical composition (wt%) of the Ti–6Al–4V alloy

Element	Al	V	Fe	N	O	H	Ti
wt%	6.41	3.93	0.16	0.008	0.18	0.0039	Bal.

The specimen used for this study comes from an (α–β) annealed 12 mm-thick rolling plate. The duplex microstructure presents a homogeneous alpha grain diameter of approx. 20 μm, and the presence of beta phase as it is shown in Fig. 1.

All the samples were machined to get the following dimensions: 15 × 11 × 1.5 mm^3. They were mechanically polished on all their faces using 4,000 grit SiC paper, and then cleaned in alcohol, and dried. All samples were weighted before and after exposure using a high precision Sartorius balance (±10 μg). Oxidations were carried out both in furnaces (under ambient air) and using SETARAM TAG24S under synthetic air. The former condition is representative of industrial thermal treatments and the latter allows us to follow oxidation kinetics and to avoid discrepancy due to laboratory humidity. The SETARAM TAG24S has the advantage of combining good accuracy with a limitation of buoyancy effects due to a symmetrical furnace in which an inert sample counterbalances these effects. Isothermal oxidation tests were carried out in 1 atm synthetic air (80 % N_2, 20 % O_2) flowing at 10 mL/min. Heating and cooling rates were set to 1 °C/s. The weight gain was continuously measured as a function of time. In this study, oxidation kinetics during isothermal tests has been analyzed following the procedure detailed in [28]. All the tested samples are presented in Table 2, along with oxidation conditions. After oxidation, all the specimens were observed with a scanning electron microscope (SEM LEO 1450 VP). Oxide scales were also characterized by X-ray diffraction (XRD) at room temperature. The data were collected in a [10–45°]Θ Bragg range with a Seifert XRD 3000 TT diffractometer in grazing 5° incidence configuration, using Cu Kα radiation, and were fitted with a diffracted-beam graphite monochromator. The phase identification uses JCPDS data files. After oxidation, cross-sections have been prepared for characterizing the oxide thickness, and for micro-hardness measurements (10 g maintained for a specific dwell time of 5 s). At least three indents have been done at different distances from the oxide scale.

Depth profiles were performed by SIMS (CAMECA IMS4F6) to obtain the oxygen distributions. Samples were characterized before and after oxidation. Surface sputtering was realized with 4.5 keV Cs+ ions, at a current density of 150 nA. Cesium was chosen in order to produce negative ions from electronegative

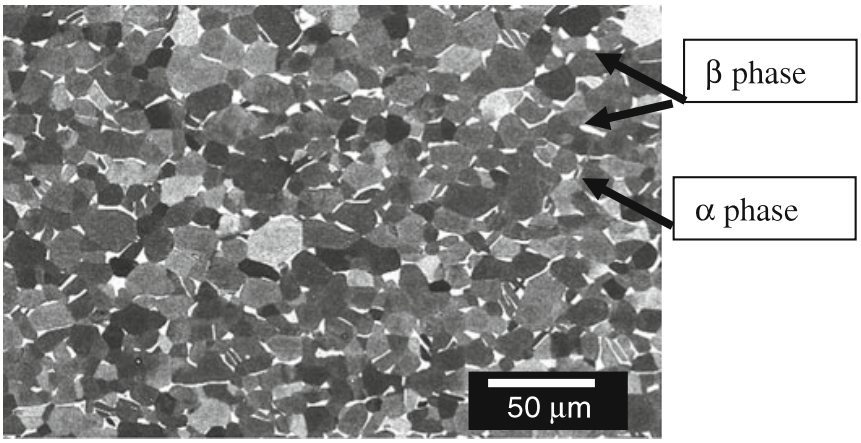

Fig. 1 Microstructure of the Ti–6Al–4V α–β annealed material

Table 2 Oxidation conditions of the samples

Specimen label	Oxidation conditions	Temperature (°C)	Duration (h)
F 600-6C	Furnace + lab air	600	6
F 650-3B	Furnace + lab air	650	3
F 650-6A	Furnace + lab air	650	6
F 700-3D	Furnace + lab air	700	3
F 750-3E	Furnace + lab air	750	3
T 650-3F	TAG24S + synthetic air	650	3
T 650-6G	TAG24S + synthetic air	650	6
T 700-3H	TAG24S + synthetic air	700	3
T 750-3I	TAG24S + synthetic air	750	3

elements such as oxygen. These experiments allow the determination of the oxygen diffusion profile in the specimen. But the development of roughness during ion sputtering is a well-known process that reduces the depth resolution of SIMS results. This was demonstrated especially for polycrystalline materials where sputtering causes roughness induced by the orientation of the grains. This point is emphasized in the studied material as it contains two different phases: hcp α-Ti and bcc β-Ti. In order to limit the sputtering impact on roughness a rotating sample holder has been developed by CAMECA. We used a rotating speed of 60 rpm. To our knowledge, SIMS analyses carried out on a rotating specimen of a two-phase polycrystalline alloy have never been published. Figure 2 shows how much roughness is reduced using this technique: for instance Ra is 3.5 and 0.7 μm only for sample F 650-6A, without and with rotation, respectively.

In order to get a good calibration of the sputtering rate for both oxidized and non-oxidized samples, precision depth measurements of shallow SIMS craters have been

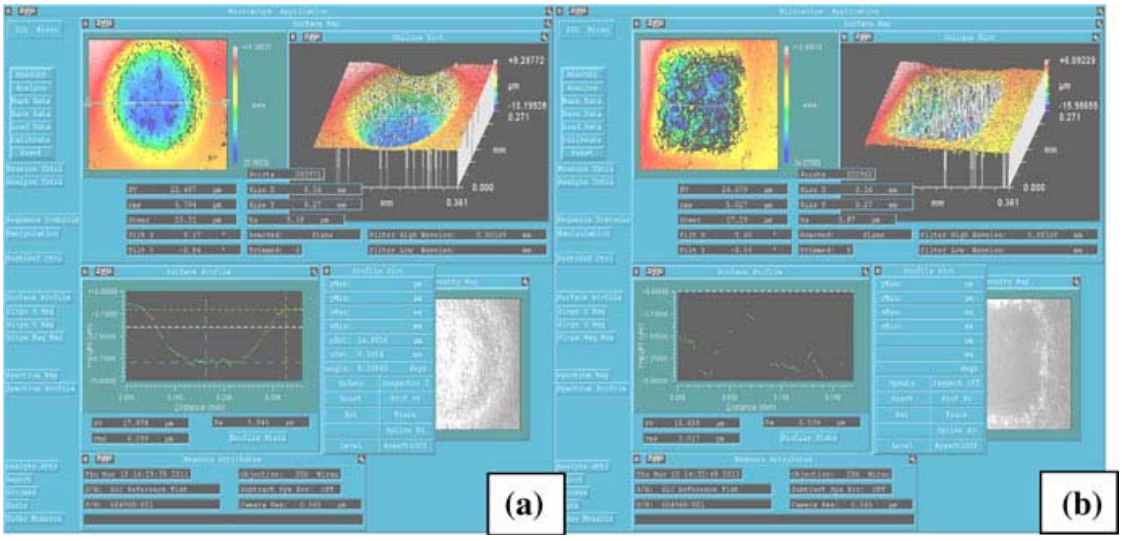

Fig. 2 F 650-6A sample oxidized at 650 °C during 6 h. Comparison between roughness measurements of the 15 μm depth sputtered hole with (**a**) (Ra = 0.7 μm) and without (**b**) rotation of the sample (Ra = 3.5 μm)

done using a ZYGO interferometer. The sputtering rate was then estimated to be 2.5 nm/s

Results

Oxide Scale

For all the samples oxidized using SETARAM TAG24, mass measurements during thermal treatments show that oxidation kinetics is parabolic as illustrated in Fig. 3. Oxidation kinetics are analyzed following the protocol explains previously [26] and the determined k_p values are given in Table 3 as well as the final net mass gains. The parabolic rate constants kp are in good agreement with the values found in the literature [16, 17, 29]. The comparison between TGA experiments and laboratory furnace oxidations reveals no significant differences in oxidation kinetics bellow 700 °C. Further experiments should be carried out at 750 °C as oxidation kinetics appears significantly reduced under laboratory air.

For all the samples the oxide scale was observed with SEM and appears adherent. XRD results indicate only TiO_2 (rutile). SEM observations of cross-sections allow us to measure oxide thickness and to perform SEM-EDX analyses. However, since the largest scale was only 2 μm, this may explain the reason why no alumina has been detected whereas it has been reported for longer oxidation duration [1]. SIMS results also corroborate oxide thickness measurements. Table 3 summarized oxide scale thicknesses measured by SEM on cross-section and using SIMS profiles. The agreement between both is good. Furthermore, it is interesting to notice that a large amount of oxygen content is not present in the oxide scale but in the titanium alloys. The proportion can be evaluated using the following hypothesis: the oxide scale is

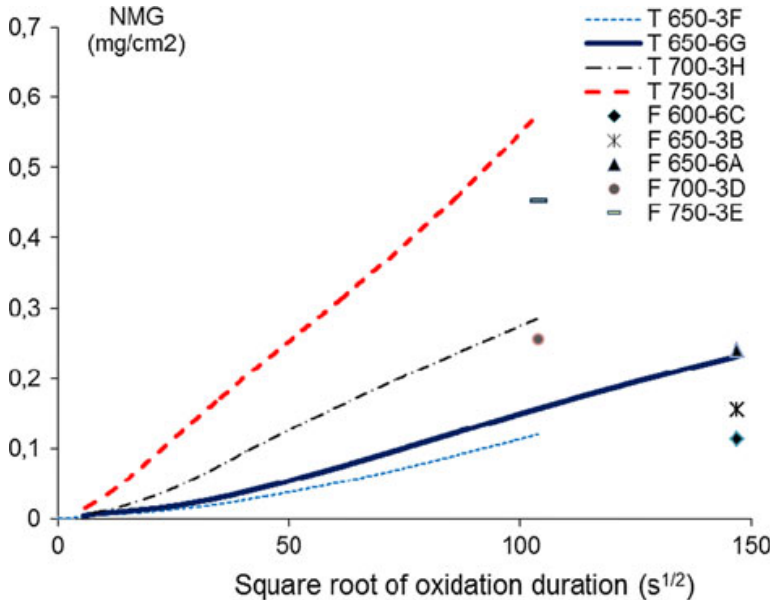

Fig. 3 Net mass gain curves during isothermal oxidation between 650 and 750 °C under synthetic air. Comparison between TGA experiments and furnace oxidations under laboratory air

Table 3 Net mass growth

Specimen label	Δm (mg/cm^2)	k_p ($mg^2\ s^{-1}\ cm^{-4}$)	Oxide thickness SEM (μm)	Oxide thickness SIMS (μm)
F 600-6C	0.112	Not calculated	1.1	1.05
F 650-3B	0.155	–	0.8	0.77
F 650-6A	0.240	–	1	1.21
F 700-3D	0.255	–	2	2.11
F 750-3E	0.453	–	2.2	2.18
T 650-3F	0.133	1.6×10^{-6}	0.6	0.45
T 650-6G	0.270	3.4×10^{-6}	0.9	0.88
T 700-3H	0.296	8.1×10^{-6}	1.1	1.07
T 750-3I	0.615	3.5×10^{-5}	2.1	2.17

fully dense with a density of 4.23 g/cm^3 and the mass gain is only due to oxygen, since no nitrogen has been found into the matrix. This last point is in good agreement with [30, 31]. The ratio of oxygen into the titanium alloy ranges from 15 to 25 % in our experiments. The proportion seems to increase with temperature and dwell time.

Oxygen Diffusion Below the Oxide Scale

When exposed to air at elevated temperatures, 300 °C or more, the oxide layer growth and the oxygen diffusion into the metal occur simultaneously. The oxygen atoms that do diffuse into the metal can occupy both interstitial and substitutional sites. This oxygen enrichment near the surface induces a greater hardness [1, 30]. Oxygen profile was measured using SIMS and micro hardness testing. The purpose was not only to evaluate oxygen diffusivity in this titanium alloy but also to use SIMS to localized oxygen in the different phases. So in the next paragraph we will first detail the results obtained from the macroscopic point of view (average oxygen content and average hardness as a function of depth from the metal oxide interface), then we will focus on the heterogeneity of the oxygen repartition. The rotation of the sample during sputtering induced a round crater (150 μm diameter) with regular slopes. The profile were achieved using the species coming from a 30 micrometers round area in the center of the crater, in the 'flat zone'. Figure 4 shows examples of chemical profiles that can be obtained.

For all profiles, reaching the oxide/alloy interface results in an abrupt change of the slope that is due to hydrogen. This property was used to segment the profile between the oxide layer and the titanium alloy substrate. So, if z stands for the distance from the surface, the distance from the metal/oxide interface was labeled x (cf. Fig. 4). Then the oxygen profile into the metal was fitted with the method described in [26], based on Fick's second law:

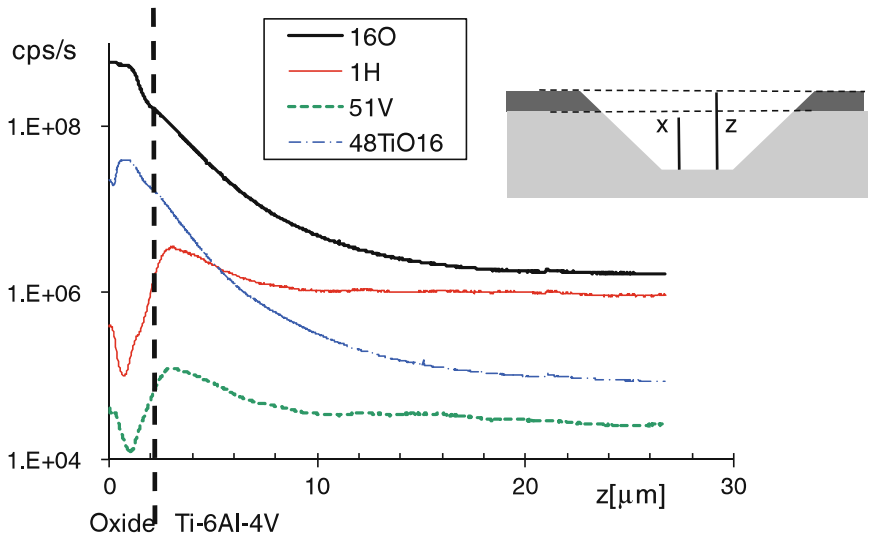

Fig. 4 SIMS profile for sample F 650-3B, z is the distance from the surface of the oxide scale (depth of the analysis), x is the distance from the metal/oxide interface. The sketch at the *top right* does not preserve the scales as the outside diameter of the crater is 150 µm

$$\frac{c - c_0}{c_s - c_0} = 1 - erf\left(\frac{x}{2\sqrt{Dt}}\right) \tag{1}$$

where c_0 is the bulk oxygen concentration c_s is the concentration at the oxide/metal interface, x is the distance from this interface, and t is the time. Concentrations were in counts per second as the expression on the left part of Eq. (1) is dimensionless. x was in cm, t in s and as a consequence D is in cm^2/s.

As SIMS sputtering lasted long enough to get stabilized oxygen signal, Eq. 1 fitted well with all the profiles as shown on Fig. 5. For each experimental condition, a diffusion coefficient was deduced from curve fit. These coefficients are

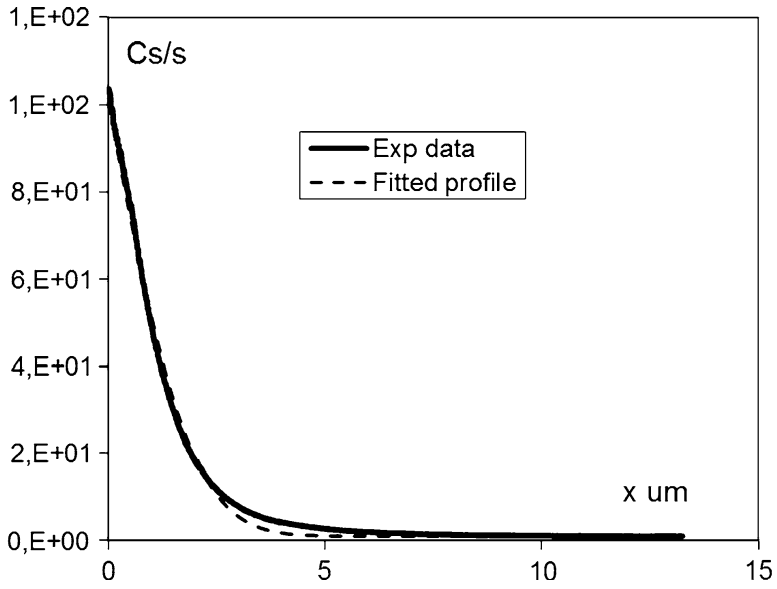

Fig. 5 (16O) SIMS profile (*black line*) and adjusted fits (*black dashed line*) for sample F 600-6C

Table 4 Diffusion coefficients obtained from curve fits

Specimen label D	(cm^2/s)
F 600-6C	8.0×10^{-13}
F 650-3B	7.3×10^{-12}
F 650-6A	5.2×10^{-12}
F 700-3D	1.1×10^{-11}
F 750-3E	1.8×10^{-11}
T 650-3F	4.5×10^{-12}
T 650-6G	5.5×10^{-12}
T 700-3H	1.0×10^{-11}
T 750-3I	2.1×10^{-11}

summarized in Table 4 and plotted on an Arrhénius diagram on Fig. 6. The activation energy for oxygen diffusion in α–β titanium, as determined with this method, is of 156 kJ/mol. The values obtained for diffusion coefficient and for activation energy are in the range of those reported in the literature [30, 32–37].

Concerning hardness measurements, the size of the indent (for the minimal load 10 g) allowed us to get a hardness profile only for sample oxidized 6 h at 650 °C, 3 h at 700 or 750 °C. Three indents were realized at each distance of the oxide interface on cross-sectioned samples for increasing value of x (see Fig. 4 for x definition). The Fig. 7 illustrated the results as well as the correlation between oxygen content and hardness. This correlation as already been reported previously for example by Göbel and coworkers in [30]

The rotation of the sample during SIMS analysis minimizes roughness. This roughness, increasing during sputtering, is due to the difference of density of the different crystallographic planes. Thanks to the sample rotation, that requires a perfect control of the apparatus as the axis of rotation of the sample must be that of the unfocused ion beam used for the ion sputtering, the slopes of the crater were regular and linear (see Fig. 2). It was then interesting to used the round and

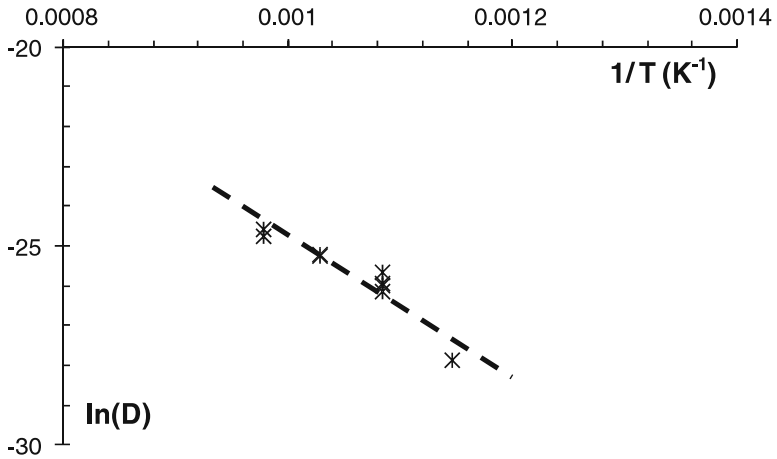

Fig. 6 Arrhenius plot of the diffusion coefficient of oxygen in Ti–6Al–4V between 600 and 750 °C

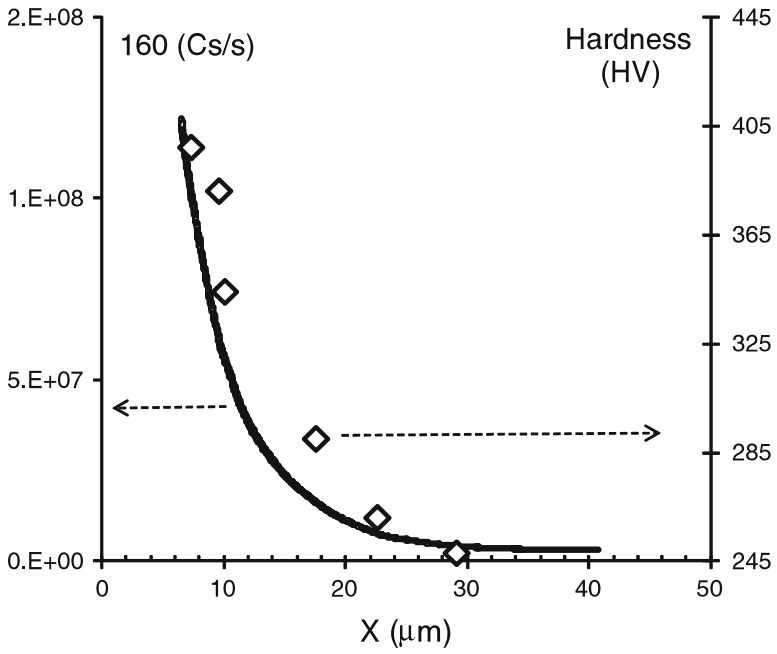

Fig. 7 Hardness measurements (*white symbol*) and oxygen profile (*dark line*) on sample T750-3I

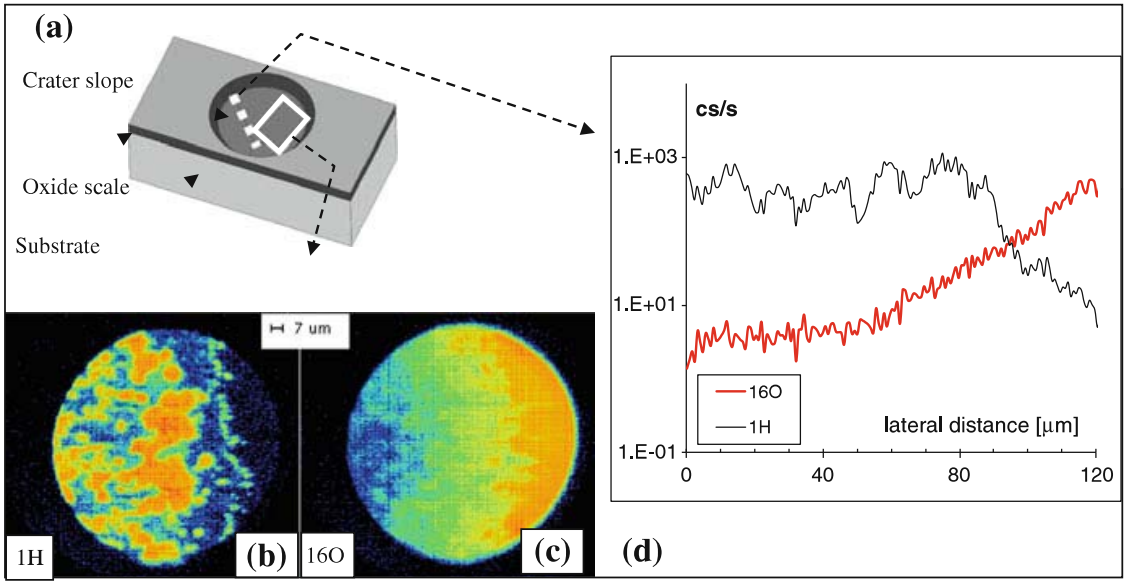

Fig. 8 SIMS mapping on the slope of a round sputtering crater of in an area rich in β phase. H is a marker of β phase. **a** schematic of the made observations **b** and **c** maps respectively of oxygen and hydrogen signals on sample F 650-6A **d** radial profile on sample F 750-3E

relatively smooth crater obtained in a mapping mode in order to focus on the heterogeneity of the chemical composition. The crater is analyzed firstly doing a chemical profile on its slope. The white dash line on Fig. 8a illustrated it and results are given on Fig. 8d. Then secondly, the mapping mode, always done on the crater slope, helps us to highlight the β phase in the α matrix as it is pointed out by the H and O maps respectively on Fig. 8b and c (the white rectangle on Fig. 8a shows the

investigated zone). Figure 8d reveals that the O profile is smoother and decreased regularly with deepness. The absence of difference in O content between α and β phase is confirmed on the O map illustrated on Fig. 8c. The H profile is not so smooth (Fig. 8d) as the O one as H is a good marker of β phase, (we cross-checked with V also) and seems in higher quantity in this phase (Fig. 8b). All the maps and the localized analyses carried out during the study did not reveal any significant enrichment in oxygen of the β phase (Fig. 8c) whereas oxygen diffusion is supposed to be enhanced in it compared to α phase. However β phase represents less than 10 volume percent of the alloy and is discontinuous. So its presence does not seem to boost oxygen diffusion.

Conclusions

Short oxidations were carried out on an α–β annealed Ti–6Al–4V in order to get data on oxidation kinetics and oxygen diffusion into the alloy. The purpose is to be able to quantify the component modification during stress relief thermal treatments. Micro hardness measurements are widely used to determine the oxidation or oxygen affected zone but not precise enough, for the lowest temperatures or the shortest oxidation. SIMS analyses on rotating specimens is investigated and allows us to get accurate data due to a decrease in differential sputtering especially in this complex or biphasic material. Compared to the scanning mode operation, SIMS with rotating specimen reduces the roughness. Then the depth of the analyzed area is less scattered. As a consequence, the precision of the oxygen profile obtained is enhanced. Furthermore, the slope of the round crater can also be used in order to get chemical maps at different depth below the oxide scale. This method allows us to get information on light elements (hydrogen and oxygen) which is not possible using EDX. Oxidation and diffusion data obtained are in good agreement with those available in the literature. Micro hardness measurements were realized for the samples with a zone affected by oxygen larger than 15 μm. A correlation was established between hardness and oxygen contents. The regular slopes of the round SIMS crater allowed us to realized chemical mapping to reveal α and β phases. Oxygen content seems to be constant at a given depth in both phases.

Acknowledgments The authors gratefully acknowledge the following students for their participation to some part of this work: Andrea Ishak Mekhail, Christophe Buirette, Virginie Dupont and Julie Voinson.

References

1. C. Leyens and M. Peters, *Titanium and Titanium Alloys*, (Wiley, Weinheim, 2003).
2. R. Boyer, G. Welsch and E. W. Collings, *Materials Properties Handbook: Titanium Alloys*, (ASM International, Materials Park, 1994), p. 148.
3. J. Alcisto, A. Enriquez, H. Garcia, S. Hinkson, M. Hahn, J. Foyos, J. Ogren, E. W. Lee and O. S. Es-Said, *Engineering Failure Analysis* **11**, 2004 (811).
4. H. L. Dua, P. K. Dattaa, D. B. Lewis and J. S. Burnell-Graya, *Corrosion Science* **36**, (4), 1994 (631).
5. I. Gurappa, *Materials Science and Engineering A* **356**, (1/2), 2003 (372).

6. W. J. Boettinger, M. E. Williams, S. R. Coriell, U. R. Kattner and B. A. Mueller, *Metallurgical and Materials Transactions B* **31B**, (6), 2000 (1419).
7. M. N. Mungole, N. Singh and G. N. Mathur, *Materials Science and Technology* **18**, (1), 2002 (111).
8. A. Galerie, M. Caillet, M. Pons and G. Dearneley, *Nuclear Instruments and Methods* **B19/20**, 1987 (708).
9. W. Kaysser, *Surface Engineering* **17**, (4), 2001 (305).
10. J. P. Riviere, L. Pichon, M. Drouet, A. Galdikas and D. Poquillon, *Surface and Coatings Technology* **200**, (18–19), 2006 (5498).
11. M. Delmas, D. Poquillon, Y. Kihn and C. Vahlas, *Surface and Coatings Technology* **200**, (5–6), 2005 (1413).
12. R. Siab, G. Bonnet, J. M. Brossard, J. Balmain and J.-F. Dinhut, *Applied Surface Science* **253**, 2007 (3425).
13. P. Kofstad, *High Temperature Corrosion*, (Elsevier, London, 1988).
14. B. Champin, L. Graff, M. Armand, G. Beranger and C. Coddet, *Journal of the Less Common Metals* **69**, 1980 (163).
15. M. Pons, M. Caillet and A. Gallerie, *Journal of the Less Common Metals* **109**, 1985 (45).
16. Y. S. Chen and C. J. Rosa, *Oxidation of Metals* **14**, 1980 (147).
17. A. M. Chaze and C. Coddet, *Oxidation of Metals* **27**, 1987 (1).
18. A. M. Chaze and C. Coddet, *Journal of the Less Common Metals* **157**, 1990 (55).
19. R. J. Hanrahan and D. P. Butt, *Oxidation of Metals* **47**, 1999 (317).
20. A. M. Chaze, C. Coddet and G. Beranger, *Journal of the Less Common Metals* **83**, 1982 (49).
21. K. Ramoul, C. Coddet, G. Beranger and F. Armanet, *Journal of the Less Common Metals* **99**, 1984 (45).
22. K. Ramoul, C. Coddet, G. Beranger and F. Armanet, *Journal of the Less Common Metals* **99**, 1984 (63).
23. A. M. Chaze and C. Coddet, *Oxidation of Metals* **21**, 1984 (205).
24. J. E. Lopes Gomes and A. M. Huntz, *Oxidation of Metals* **14**, 1980 (249).
25. A. M. Chaze and C. Coddet, *Oxidation of Metals* **28**, 1988 (61).
26. P. Perez, V. A. C. Haanappel and M. F. Stroosnijder, *Oxidation of Metals* **53**, 2000 (481).
27. S. R. J. Saunders, M. Monteiro and F. Rizzo, *Progress in Materials Science* **53**, (5), 2008 (775).
28. D. Monceau and B. Pieraggi, *Oxidation of Metals* **50**, (5/6), 1998 (477).
29. P. Kofstad, *High Temperature Oxidation of Metals*, (Wiley, New York, 1966).
30. M. Göbel, V. A. C. Haanappel and M. F. Stroosnijder, *Oxidation of Metals* **55**, (1/2), 2001 (137).
31. C. Schuman, E. Lenarduzzi, S. Weber, M. J. Philippe, D. Petelot and P. Bounie, *Surface and Coatings Technology* **200**, 2006 (4572).
32. C. J. Rosa, *Metallurgical and Materials Transactions* **1**, 1970 (2517).
33. A P. Broumas, N. M. Degnan, M. L. Meier, Proceedings of the American Society for Engineering Education Annual Conference and Exposition, Session 3264, Nashville (2003).
34. D. Gupta and S. Weinig, *Acta Metallurgica* **10**, 1962 (292).
35. J. N. Pratt, W. J. Bratina and B. Chalmers, *Acta Metallurgica* **2**, 1954 (203).
36. F. Guillemot, J. Debuigne and D. Ansel, *Comptes Rendus de l'Académie des Sciences—IIC* **4**, (5), 2001 (381).
37. W. P. Roe, H. R. Palmer and W. R. Opie, *Transactions ASM* **52**, 1960 (191).